Biaxially Textured YBa$_2$Cu$_3$O$_{7-x}$ Microwave Cavity in a High Magnetic Field for a Dark-Matter Axion Search

Danho Ahn[⊙],[1,2] Ohjoon Kwon,[2] Woohyun Chung[⊙],[2,*] Wonjun Jang,[3,†] Doyu Lee,[2,‡] Jhinhwan Lee,[4] Sung Woo Youn[⊙],[2] HeeSu Byun,[2] Dojun Youm,[1] and Yannis K. Semertzidis[1,2]

[1]*Department of Physics, Korea Advanced Institute of Science and Technology (KAIST), Daejeon 34141, Republic of Korea*

[2]*Center for Axion and Precision Physics Research, Institute for Basic Science, Daejeon 34051, Republic of Korea*

[3]*Center for Quantum Nanoscience, Institute for Basic Science, Seoul 33760, Republic of Korea*

[4]*Center for Artificial Low Dimensional Electronic Systems, Institute for Basic Science, Pohang 37673, Republic of Korea*

A high-quality (Q)-factor microwave resonator in the presence of a strong magnetic field can have a wide range of applications, such as in axion dark matter searches where the two aspects must coexist to enhance the experimental sensitivity. We introduce a polygon-shaped cavity design with biaxially textured YBa$_2$Cu$_3$O$_{7-x}$ superconducting tapes covering the entire inner wall. Using a 12-sided polygon cavity, we obtain substantially improved Q factors of the 6.9-GHz TM$_{010}$ mode at 4 K with respect to a copper cavity and observe no considerable degradation in the presence of magnetic fields up to 8 T.

The advancement of superconducting radio-frequency (SRF) technology allows a rf resonator to obtain an extremely high quality (Q) factor and to be used in a broad scope of applications [1–4]. However, the requirement of an external magnetic field could limit scientific productivity in many areas where a strong external magnetic field is absolutely necessary. Examples include the beam screen design at the future circular collider [5,6] and high-Q-factor cavities in axion dark matter and axionlike particle searches [7–11]. In particular, the axion dark matter detection scheme proposed by Sikivie [12,13] utilizes a resonant cavity immersed in a strong magnetic field (>7 T) [14–18], by which axions are converted into microwave photons [Fig. 1(a)]. Obtaining a high Q factor in a strong magnetic field will profoundly impact the way axion dark matter experiments are performed. It will substantially increase the axion-to-photon conversion power [19] with expected Q factors of about that of axions (approximately 10^6) [20] and will permit investigations of the detailed axion signal structure in the frequency domain. Furthermore, achieving a quality factor of more than 10^8 can open a window for ultranarrow-axion-linewidth research for different galactic structures of axion dark matter [21].

Recently, the high-frequency responses of biaxially textured, second-generation rare-earth barium copper oxide (REBa$_2$Cu$_3$O$_{7-x}$, REBCO) coated conductors (CCs) [Fig. 1(b)] were studied in high magnetic fields up to 16 T for the beam screen of the future circular hadron-hadron collider [22]. For an ideal cylindrical cavity with a CC surface, the Q factor can be expected to be at least 10^6. Considering the typical experimental conditions in dark matter axion search, the Q factor could be larger, because vortex pinning becomes stronger at lower temperature (100 mK) and in a magnetic field parallel to a REBCO film [23–25]. A high depinning frequency (>10 GHz) is also favorable for a dark matter axion search with target frequency ranges up to 100 GHz.

Fabricating a three-dimensional (3D) resonant cavity structure with a second-generation REBCO film poses large technical challenges because of its biaxial texture. Directly forming a biaxially textured REBCO film on the deeply concaved inner surface of a cavity is difficult because of the limitations in making well-textured buffer layers and substrate [26–29]. A possible solution to this problem is to implement a 3D surface with two-dimensional planar objects. We take advantage of high-grade, commercially available YBa$_2$Cu$_3$O$_{7-x}$ (YBCO) tapes from American Superconductor, whose fabrication process, structure, and properties are well known [30]. The substrate and buffer layers of the tape are designed to act as template layers to provide a biaxial texture to the YBCO film. The film architecture of the tape

---

*gnuhcw@ibs.re.kr

†Present address: Samsung Advanced Institute of Technology, Suwon 16678, Republic of Korea.

‡Present address: Samsung Electronics, Hwaseong 18448, Republic of Korea.
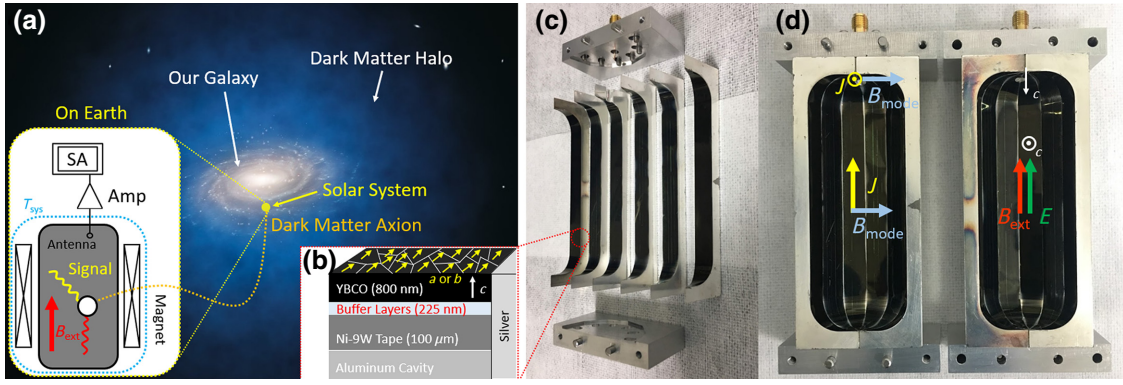
FIG. 1.   (a) A schematic of the axion haloscope illustrates the dark matter axion (dotted green line) in the dark matter halo (credit: ESO/L. Calçada) converts to a gigahertz rf signal (curved yellow line) in the resonant cavity (gray box) via interaction with an external dc magnetic field (red arrow and curved red line, B_{ext}) from the magnet (white boxes with a cross). The cavity is installed in a cryogenic system (dotted blue box) with a system temperature (T_{sys}). A signal collected by an antenna is detected by the spectrum analyzer (white box with "SA") after passing the amplifier (white triangle). (b) Schematic of the cross section of a cavity piece shows the structure of the various layers (YBCO, buffer layers, nickel-tungsten) and the silver layer on the aluminum cavity. The c axis of the YBCO crystal (white arrow) and the a or b axis of the single-crystal YBCO grains (yellow arrows) are represented. (c) Six aluminum cavity pieces; a YBCO tape is attached to each. (d) Twelve pieces (two cylinder halves) are assembled to make a whole cavity. The magnetic fields of a TM_{010} mode (left, blue arrows) on the inner surface (black area) point in the vertical direction of the gap between the pieces. The surface current directions (left, yellow arrow and circle) are parallel to the gap direction. The c axes of the YBCO grains (right, white arrow and circle) are vertical to the tape surface. At the middle of the cavity, the electric fields of the TM_{010} mode (right, green arrow), which maximize the axion-to-photon conversion power, are parallel to the external magnetic field (right, red arrow).

consists of the following layers. On 100-μm biaxially textured 9% nickel-tungsten (Ni-9W) alloy, 800-nm-thick YBCO is deposited on top of the buffer layers that consist of yttrium oxide (Y_2O_3), yttria-stabilized zirconia (YSZ), cerium oxide (CeO_2), which are each 75 nm thick [Fig. 1(b)].

To realize a 3D superconducting cavity for axion search utilizing YBCO tapes, we devise a 12-piece polygon cavity to which biaxially textured tapes are attached [Fig. 1(b)]. Each tape is attached securely to the inner surface of a cavity wedge. By removing the silver protective layers from the tape, the inner wall of each wedge is fully covered with a single YBCO film. The idea behind this design is to cover the entire inner surface with superconducting tapes.

A polygon cavity design is adopted considering the cavity mode used in dark matter axion search. The signal power ($P_{a\gamma\to\gamma}$) through a cavity in the experiment [Fig. 1(a)] is given by [19]

$$P_{a\gamma\to\gamma} = g_{a\gamma\gamma}^2 \frac{\rho_a}{m_a^2} B_{ext}^2 V \omega_0 C \frac{Q_c Q_a}{Q_c + Q_a}, \quad (1)$$

relating the coupling constant ($g_{a\gamma\gamma}$), the density of dark matter axions (ρ_a), the rest mass of axions (m_a), the Q factor of the axion signal ($Q_a \sim 10^6$), the volume average of a square of external magnetic field (B_{ext}^2), and the properties of a cavity, which are the volume (V), the resonant frequency (ω_0), the Q factor (Q_c), and the form factor (C). The formula shows that the signal power is affected by the form factor as well as the Q factor. The form factor for

the given electric and electric displacement fields of a resonant mode ($\mathbf{E}$, $\mathbf{D}$) [Fig. 1(d)] and the vacuum magnetic susceptibility (μ_0) is [19]

$$C = \frac{\mu_0 \left(\int \mathbf{E} \cdot \mathbf{B}_{ext} dV\right)^2}{B_{ext}^2 V \int \mathbf{D} \cdot \mathbf{E} dV}. \quad (2)$$

The equation has a maximized value at TM_{010} mode ($C_{cy} \sim 0.69$) where its electric fields and external magnetic fields are parallel in the z direction in a cylindrical cavity. Eigenmode analysis using COMSOL MULTIPHYSICS version 5.2 [31,32] shows that both the form factor and Q factor of a polygon cavity with perfectly connected surfaces are comparable with those of a cylindrical cavity ($\Delta Q/Q < 5\%$, $C_{pol} \sim 0.67$).

The polygon cavity does not cause any significant degradation of the cavity performance due to electromagnetic wave propagation through the gaps between the wedges. In simulation, with perfectly conducting surfaces, the cavity Q factor is maintained at 10^7 even with large gaps (100 μm), and the Q factor increases as gaps become smaller. This is because the gaps do not allow wave propagation from the TM_{010} mode. Only a very weak evanescent field can exist there (see the Supplemental Material [33]). For the same reason, the cavity form factor also maintains its value within 1% degradation even with the gaps ($C_{pol+gaps} \sim 0.67$).

The prototype cavity is fabricated as follows. The tape is attached with 10-mm minimum bending [34] to prevent

cracks on the YBCO film. The edges of the tape are polished so that the edges fit the sides of a wedge. Once the YBCO tape is completely attached to the inner surface of each polygon piece, we remove the silver protective layers to expose the bare YBCO surface using a mixture of hydrogen peroxide and 60% ammonium water with a 1:1 volume ratio.

The cut edges of the YBCO tape exposed on the side are coated by sputtering silver to avoid potential rf loss due to the layers behind the YBCO film [Fig. 1(b)]. The target thickness of the film is 2 μm. We control the deposition time based on film thickness measurements using a quartz crystal microbalance [35]. During the sputtering, the main surfaces of the YBCO tape are masked. The penetration of silver at the YBCO surface edge is as much as 50 μm as determined from optical microscopy.

The assembly mechanism is designed to reduce the gap size. The alignment of the wedges is facilitated by precision alignment pins located on the top and bottom of the cavity [Fig. 1(d)]. The wedges are also tightened using seven c-clamps. Inspection with optical microscopy ensures the gap size is around 20 μm. The assembled cavity is installed in a cryogen-free dilution refrigerator, BF-LD400 [36], equipped with an 8-T NbTi superconductor solenoid [37], and brought to a low temperature of around 4 K [Fig. 1(a)]. The Q factor and resonant frequency are measured using a network analyzer through a transmission signal between a pair of rf antennae, which are weakly coupled to the cavity. The coupling strengths of the antennae are monitored throughout the experiment
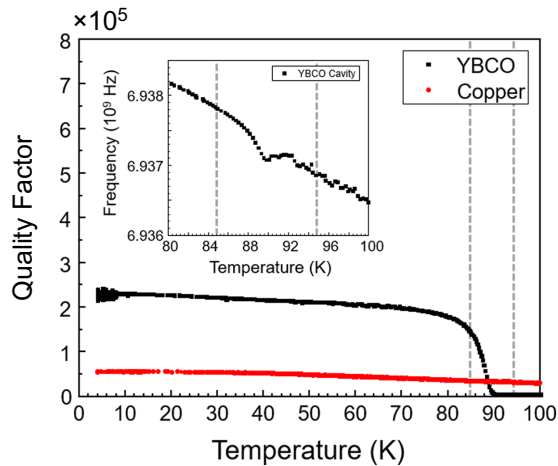

FIG. 3. The measurement results of the 12-piece polygon cavities: Q factor versus external magnetic field from 0 to 8 T. The vertical dashed line shows the magnetic field of 0.23 T at which the abrupt Q-factor enhancement starts. The maximum Q factor is around 335 000.

FIG. 2. The measurement results of the 12-piece polygon cavities: Q factor versus temperature from 4.2 to 100 K. The black dots are for the YBCO cavity and the red dots are for the copper cavity with the same polygon geometry. The inset plot is resonant frequency versus temperature from 80 to 100 K. The phase transition from normal metal to superconductor starts near 90 K, at which an anomalous frequency shift occurs. The vertical gray dashed lines indicate temperatures of 85 and 95 K.
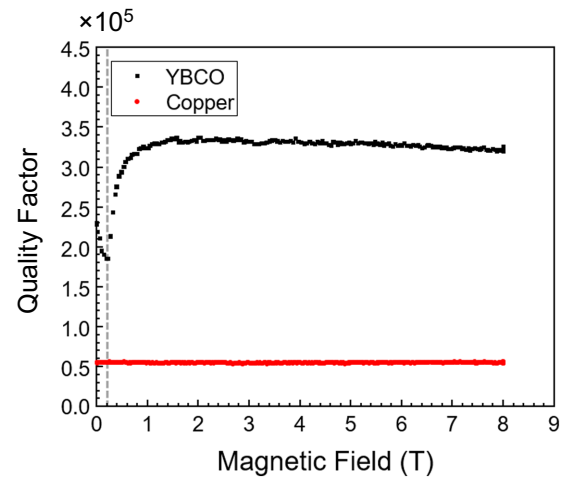
and accounted for in obtaining the unloaded quality factor. Measuring the Q factor (TM$_{010}$ mode) of the polygon cavity with 12 YBCO pieces by varying the temperature, we observe the superconducting phase transition at around 90 K, which is in agreement with the critical temperature (T_c) of YBCO (Fig. 2). The global increase in the resonant frequency is due to thermal shrinkage of the aluminum cavity, but an anomalous frequency shift is also observed near the critical temperature. The decrease in the frequency shift at T_c can be attributed to the divergence of the penetration depth of the YBCO surface [23]. The maximum Q factor at 4.2 K is about 220 000. The Q factor for a polygon cavity made of pure (oxygen-free, high-thermal-conductivity) copper with the same geometry is measured to be 55 500 at the same temperature. Varying the applied dc magnetic field from 0 to 8 T, at the initial ramping up of the magnet, the Q factor of the cavity drops rapidly to 180 000 until the magnetic field reaches 0.23 T and then rises to the maximum value of 335 000, which is about 6 times higher than that of a copper cavity, at around 1.5 T for the TM$_{010}$ mode. From the measurement, we observe that the Q factor of the resonant cavity's TM$_{010}$ mode does not decrease significantly (changing only a few percent) up to 8 T (Fig. 3).

The abrupt behavior of Q factors near 0.23 T is investigated using a 12-piece Cu cavity with single silver-etched tape attached to only one piece. The tape is attached to a copper cavity wedge exposing the back side, which is a clean Ni-9W surface. The conductivity of copper does not change much under a magnetic field (Fig. 3), and thus the Q-factor change between 0 and 3 T depends on the surface resistance of Ni-9W (Fig. 4). A comparison
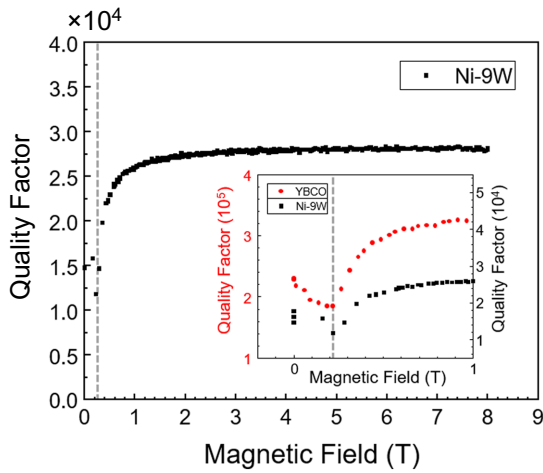
FIG. 4. Measurement related to the nickel-tungsten alloy: Q factor versus external magnetic field for the 12-piece copper polygon cavity with one piece of Ni-9W (from 0 to 8 T at 4 K). The Q-factor behavior is the same as in the YBCO cavity. There is an abrupt change of the Q factor at 0.23 T.
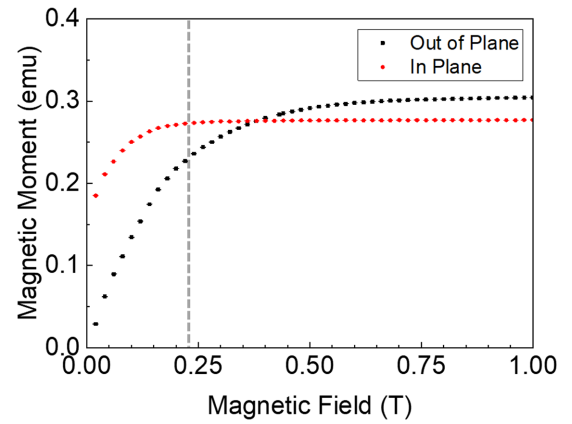

FIG. 5. Measurement related to the nickel-tungsten alloy: the magnetization curve for the Ni-9W tape (4×4 mm). The magnetic saturation of the Ni-9W tape, which is aligned with the in-plane direction of the dc magnetic field, almost ends at 0.23 T at which the Q factor of the YBCO cavity is abruptly changed. The vertical dashed line represents 0.23 T. For the out-of-plane case, the magnetic saturation ends at around 1 T at which the Q factor of the YBCO cavity is saturated.

between the YBCO cavity and the Ni-9W cavity clearly shows that the unexpected change in Q factor near 0.23 T is caused by the Ni-9W layer behind the YBCO layer. Furthermore, we also measure the magnetization of a small Ni-9W piece (4×4 mm) in a magnetic property measurement system (Quantum Design MPMS3-Evercool [38]) with in-plane and out-of-plane alignments (parallel and perpendicular to the applied magnetic field, respectively) to investigate where the saturation occurs. Nitric acid is used to etch the YBCO film on the 4×4 mm tape. The sample is installed in the equipment with a straw so that the rectangular sample can be aligned in any direction by hand. The measurements show that the magnetic saturation of the in-plane (out-of-plane) Ni-9W ends near 0.23 T (1.0 T) (Fig. 5). The magnetic saturation lowers the surface resistance, because the atomic spins become more rigid due to the reduction of the magnetic domain walls. In other words, the Q factor is suddenly increased at 0.23 T because the main surface loss originates from the side wall, which is aligned in the in-plane direction with the external field. After that, the other surfaces are saturated until 1.0 T, where the Q factor of the YBCO cavity is maximum. Those studies indicate that Ni-9W is the dominant source of energy loss in the polygon cavity. This is supported by the simulation result that a small amount of Ni-9W defects exposed by cracks and over-etched YBCO surface could degrade a Q factor to the order of 10^5 [39–42] (see Supplemental Material [33]).

The maximum Q factor achievable with a REBCO cavity is currently unknown, but a comparison between the surface resistance of copper (approximately 5 mΩ, 7 GHz) and YBCO at 4 K (<0.2 mΩ, 7 GHz with an 8-T field

parallel to the c axis) [22–25] suggests that the Q factor could be as much as 25 times higher than that of a copper cavity even with a strong magnetic field present. In the near future, improvements are expected using techniques to expose the bare YBCO surface from the tape, eventually reducing the area where surface losses occur inside the cavity. Moreover, if the layer that creates a large energy loss, such as Ni-9W, can be eliminated or covered completely, we can expect a much higher Q factor. Our design of the vertically split, polygon cavity to implement biaxially textured YBCO on the inner surface allows us to test the potential of superconducting resonant cavities that could be used in a strong magnetic field. We have demonstrated that it is possible to fabricate a cavity with a YBCO inner surface to maintain a high Q factor at up to 8 T. This result could not only eliminate a significant limitation of SRF applications with a magnetic fields in many areas, but also provide us with a tool for an enhanced dark matter axion search.

[1] P. Camgagne-Ibarcq, A. Eickbusch, S. Touzard, E. Zalys-Geller, N. E. Frattini, V. V. Sivak, P. Reinhold, S. Puri, S. Shankar, R. J. Schoelkopf, L. Frunzio, M. Mirrahimi, and M. H. Devoret, Quantum error correction of a qubit encoded in grid states of an oscillator, Nature **584,** 368 (2020).

[2] M. Reagor, W. Pfaff, C. Axline, R. W. Heeres, N. Ofek, K. Sliwa, E. Holland, C. Wang, J. Blumoff, K. Chou, M. J. Hatridge, L. Frunzio, M. H. Devoret, L. Jiang, and R. J. Schoelkopf, Quantum memory with millisecond coherence in circuit QED, Phys. Rev. B **94,** 014506 (2016).

[3] H. Padamsee, The science and technology of superconducting cavities for accelerators, Supercond. Sci. Technol. **14,** R28 (2001).

[4] H. Padamsee, 50 years of success for SRF accelerators—A review, Supercond. Sci. Technol. **30,** 1 (2017).

[5] S. Calatroni, E. Bellingeri, C. Ferdeghini, M. Putti, R. Vaglio, T. Baumgartner, and M. Eisterer, Thallium-based high-temperature superconductors for beam impedance mitigation in the Future Circular Collider, Supercond. Sci. Tech. **30,** 1 (2017).

[6] R. Vaglio and S. Calatroni, Advances in the study of HTS superconductors for the beam impedance mitigation in CERN-FCC: The thermal runaway problem, Eur. Phys. J. Spec. Top. **228,** 749 (2019).

[7] T. M. Shokair, J. Root, K. A. Van Bibber, B. Brubaker, Y. V. Gurevich, S. B. Cahn, S. K. Lamoreaux, M. A. Anil, K. W. Lehnert, B. K. Mitchell, A. Reed, and G. Carosi, Future directions in the microwave cavity search for dark matter axions, Int. J. Mod. Phys. A **29,** 1443004 (2014).

[8] D. Alesini, *et al.*, Galactic axions search with a superconducting resonant cavity, Phys. Rev. D **99,** 101101(R) (2019).

[9] R. Janish, V. Narayan, S. Rajendran, and P. Riggins, Axion production and detection with superconducting rf cavities, Phys. Rev. D **100,** 015036 (2019).

[10] Z. Bogorad, A. Hook, Y. Kahn, and Y. Soreq, Probing Axionlike Particles and the Axiverse with Superconducting Radio-Frequency Cavities, Phys. Rev. Lett. **123,** 021801 (2019).

[11] A. Berlin, R. T. D'Agnolo, S. A. R. Ellis, C. Nantista, J. Neilson, P. Schuster, N. Roro, and K. Zhou, Axion dark matter detection by superconducting resonant frequency conversion, J. High Energy Phys. **2020,** 88 (2020).

[12] P. Sikivie, Experimental Tests of the Invisible Axion, Phys. Rev. Lett. **51,** 1415 (1983).

[13] P. Sikivie, Detection rates for invisible-axion searches, Phys. Rev. D **32,** 2988 (1985).

[14] T. Braine, *et al.*, Extended Search for the Invisible Axion with the Axion Dark Matter Experiment, Phys. Rev. Lett. **124,** 101303 (2020).

[15] K. M. Backes, *et al.*, A quantum enhanced search for dark matter axions, Nature **590,** 238 (2020).

[16] O. Kwon, *et al.*, First Results from an Axion Haloscope at CAPP around 10.7 μeV, Phys. Rev. Lett. **126,** 1981802 (2021).

[17] S. Lee, S. Ahn, J. Choi, B. R. Ko, and Y. K. Semertzidis, Axion Dark Matter Search around 6.7 μeV, Phys. Rev. Lett. **124,** 101802 (2020).

[18] J. Hong, J. E. Kim, S. Nam, and Y. K. Semertzidis, eprint: arXiv:1403.1576.

[19] D. Kim, J. Jeong, S. W. Youn, Y. Kim, and Y. K. Semertzidis, Revisiting the detection rate for axion haloscopes, JCAP **2020,** 66 (2020).

[20] M. S. Turner, Periodic signatures for the detection of cosmic axions, Phys. Rev. D **42,** 3572 (1990).

[21] J. Hoskins, J. Hwang, C. Martin, P. Sikivie, N. S. Sullivan, D. B. Tanner, M. Hotz, L. J. Rosenberg, G. Rybka, A. Wagner, S. J. Asztalos, G. Carosi, C. Hagmann, D. Kinion, K. van Bibber, R. Bradley, and J. Clarke, Search for non-virialized axionic dark matter, Phys. Rev. D **84,** 121302(R) (2011).

[22] A. Romanov, P. Krkotić, G. Telles, J. O'Callaghan, M. Pont, F. Perez, X. Granados, S. Calatroni, T. Puig, and J. Gutierrez, High frequency response of thick REBCO coated conductors in the framework of the FCC study, Sci. Rep. **10,** 12325 (2020).

[23] M. Golosovsky, M. Tsindlekht, H. Chayet, and D. Davidov, Vortex depinning frequency in YBa$_2$Cu$_3$O$_{7-x}$ superconducting thin films: Anisotropy and temperature dependence, Phys. Rev. B **50,** 470 (1994).

[24] M. Golosovsky, M. Tsindlekht, and D. Davidov, High-frequency vortex dynamics in YBa$_2$Cu$_3$O$_7$, Supercond. Sci. Technol. **9,** 1 (1996).

[25] S. Revenaz, D. E. Oates, D. Labbé-Lavigne, G. Dresselhaus, and M. S. Dresselhaus, Frequency dependence of the surface impedance of YBa$_2$Cu$_3$O$_{7-\delta}$ thin films in a dc magnetic field: Investigation of vortex dynamics, Phys. Rev. B **50,** 1178 (1994).

[26] D. P. Norton, A. Goyal, J. D. Budai, D. K. Christen, D. M. Kroeger, E. D. Specht, Q. He, B. Saffian, M. Paranthaman, C. E. Klabunde, D. F. Lee, B. C. Sales, and F. A. List, Epitaxial YBa$_2$Cu$_3$O$_7$ on biaxially textured nickel (001): An approach to superconducting tapes with high critical current density, Science **274,** 755 (1996).

[27] Q. Li, W. Zhang, U. Schoop, M. W. Rupich, S. Annavarapu, D. T. Verebelyi, C. L. H. Thieme, V. Prunier, X. Cui, M. D. Teplitsky, L. G. Fritzemeier, G. N. Riley, M. Paranthaman, A. Goyal, D. F. Lee, and T. G. Holesinger, Progress in solution-based YBCO coated conductor, Physica C **357–360,** 987 (2001).

[28] R. P. Reade, P. Berdahl, and R. E. Russo, Ion-beam nanotexturing of buffer layers for near-single-crystal thin-film deposition: Application to YBa$_2$Cu$_3$O$_7 - \delta$ superconducting films, Appl. Phys. Lett. **80,** 1352 (2002).

[29] C. Rey, *Superconductors in the Power Grid Ch. 4* (Elsevier, Cambridge, United Kingdom, 2015).

[30] X. Li, M. W. Rupich, C. L. H. Thieme, M. Teplitsky, Srivatsan Sathyamurthy, E. Thompson, D. Buczek, J. Schreiber, K. DeMoranville, J. Lynch, J. Inch, D. Tucker, R. Savoy, and S. Fleshler, The development of second generation HTS wire at American Superconductor, IEEE Trans. Appl. Supercond. **19,** 3231 (2009).

[31] www.comsol.com.

[32] J. D. Jackson, *Classical Electrodynamics* (John Wiley & Sons, Hoboken, 2007).

[33] See Supplemental Material at http://link.aps.org/supplemental/10.1103/PhysRevApplied.17.L061005 for detailed simulation results for a polygon cavity with gaps.

[34] V. Solovyov and P. Farrell, Exfoliated YBCO filaments for second-generation superconducting cable, Supercond. Sci. Technol. **30,** 1 (2017).

[35] www.inficon.com/en/products/qcm-crystals.

[36] www.bluefors.com.

[37] www.americanmagnetics.com.

[38] www.qdusa.com.

[39] R. G. Chambers, Anomalous skin effect in metals, Nature **165**, 239 (1950).

[40] S. Calatroni, M. Arzeo, S. Aull, M. Himmerlich, P. C. Pinto, W. Vollenberg, B. Di Girolamo, P. Cruikshank, and P. Chiggiato, Cryogenic surface resistance of copper: Investigation of the impact of surface treatments for secondary elec-

tron yield reduction, Phys. Rev. Accel. Beams **22**, 063101 (2019).

[41] K. Jin, B. C. Sales, G. M. Stocks, G. D. Samolyuk, M. Daene, W. J. Weber, Y. Zhang, and H. Bei, Tailoring the physical properties of Ni-based single-phase equiatomic alloys by modifying the chemical complexity, Sci. Rep. **6**, 20159 (2016).

[42] A. F. Clark, G. E. Childs, and G. H. Wallace, Electrical resistivity of some engineering alloys at low temperatures, Cryogenics **10**, 295 (1970).